OBSERVATIONS OF SHORT-RANGE WAKEFIELD EFFECTS IN TESLA-TYPE SUPERCONDUCTING RF CAVITIES*

A.H. Lumpkin[#], R. Thurman-Keup, D. Edstrom Jr., J. Ruan
Fermi National Accelerator Laboratory, Batavia, IL 60510 USA

Abstract

The Fermilab Accelerator Science and Technology (FAST) facility has a unique configuration of a photocathode rf gun beam injecting two TESLA-type single cavities (CC1 and CC2) in series prior to the cryomodule. To investigate short-range wakefield effects, we have steered the beam to minimize the signals in the higher-order mode (HOM) detectors of CC1 and CC2 for a baseline, and then used a vertical corrector between the two cavities to steer the beam off axis at an angle into CC2. A Hamamatsu synchroscan streak camera viewing a downstream OTR screen provided an image of y-t effects within the micropulses with ~10-micron spatial resolution and 2-ps temporal resolution. At 500 pC/b, 50 b, and 4 mrad off-axis steering into CC2, we observed an ~ 100-micron head-tail centroid shift in the streak camera image y(t)-profiles. This centroid shift value is 5 times larger than the observed HOM-driven centroid oscillation within the macropulse and is consistent with a calculated short-range wakefield effect. Additional results for kick-angle compensations will be presented.

INTRODUCTION

The accelerators for high-power x-ray free-electron laser (FEL) facilities such as the European XFEL [1] and planned LCLS-II x-ray FEL [2] are employing TESLA-type SCRF cavities. Beam propagation off axis in these cavities can result in both short-range and long-range transverse wakefields which can lead to emittance dilution within the micropulses and macropulses, respectively. There are limited beam-effects data available, although we recently reported the clear observations of submacropulse beam centroid oscillation effects due to the long-range effects of HOMs [3].

We report here sub-micropulse effects on beam transverse position centroids and sizes correlated with off-axis beam steering in TESLA-type cavities at the Fermilab Accelerator Science and Technology (FAST) Facility [4]. We used a 3-MHz micropulse repetition rate, a unique two separated-single-cavity configuration, and targeted diagnostics for these tests. Our initial data from an optical transition radiation (OTR) imaging source indicated our streak camera can provide ~10-micron spatial resolution with 1-2 ps (σ) temporal resolution depending on the bandpass filter employed. Since the observed bunch lengths were 10-15 ps (σ), we had sufficient resolution for

up to 20 time slices in the 4σ profile. In this sense we also obtained slice-emittance information. We used the HOM detectors and rf BPMs to assess our off-axis steering to generate and then evaluate the short-range wakefield effects on the beam dynamics.

EXPERIMENTAL ASPECTS

The FAST Injector Linac

The FAST linac is based on the L-band rf photocathode (PC) gun which injects beam into two superconducting rf (SCRF) capture cavities denoted CC1 and CC2, followed by transport to a low-energy electron spectrometer. A Cs_2Te photocathode is irradiated by the UV component of the drive laser system described elsewhere [5]. The basic diagnostics for the studies include the rf BPMs located before, between, and after the two cavities as shown in Fig. 1. These are supplemented by the imaging screens at X107, X108, X121, and X124. The HOM couplers are located at the upstream and downstream ends of each SCRF cavity, and these signals are processed by the HOM detector circuits with the output provided online though ACNET, the Fermilab accelerator controls network. The HOM detectors' bandpass filters were optimized for two dipole passbands from 1.6 to 1.9 GHz, and the 1.3 GHz fundamental was reduced with a notch filter. The rf BPMs electronics were configured for bunch-by-bunch capability with reduced noise. At 2 nC per micropulse, the rms noise was found to be 25 µm in the horizontal axis (x) and 15 µm in the vertical axis (y) in B101 in the test with 4.5-MeV beam from the gun. However, for these experiments on short-range transverse wakefields, we relied on a streak camera to provide the sub-micropulse spatial information.

The Streak Camera System

We utilized a C5680 Hamamatsu streak camera with S20 PC operating with the M5675 synchroscan vertical deflection unit that was phase locked to 81.25 MHz. In addition, we used a phase-locked-loop C6878 delay box that stabilizes the streak image positions to about 1 ps temporal jitter over 10s of minutes. These steps enabled the synchronous summing of 50-150 micropulses or bunches (b) generated at 3 MHz by the photoinjector or the offline summing of 10-100 images to improve statistics in the sum images. We applied the principle to optical transition radiation (OTR) generated from an Al-coated Si substrate at the X121 screen location (see Fig.1) with subsequent transport to the beamline streak camera. Commissioning of the streak camera system was facilitated through a suite of
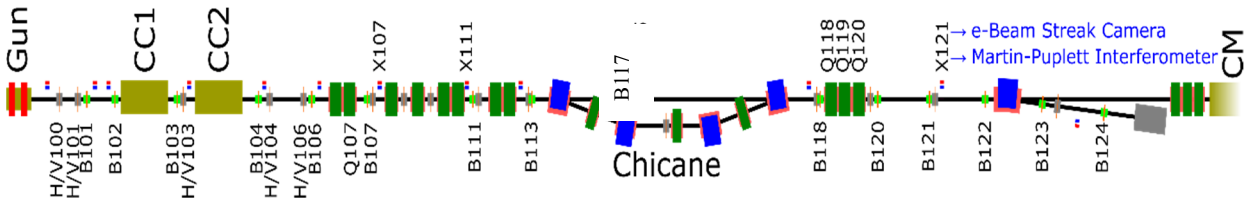
Figure 1: Schematic of the FAST beamline layout showing the capture cavities, correctors, rf BPMs, chicane, X121 OTR screen, spectrometer, and the beginning of the cryomodule (CM).

controls centered around ACNET. This suite includes operational drivers to control and monitor the streak camera as well as Synoptic displays to facilitate interface with the driver. Images are captured from the streak camera using the readout camera, Prosilica 1.3 Mpixel cameras with 2/3" format, and may be analyzed both online with a Java-based ImageTool and an offline MATLAB-based ImageTool processing program [6,7]. Bunch-length measurements using these techniques have been reported previously from the A0 Facility [8] and FAST first system streak camera commissioning at 20 MeV [9].

EXPERIMENTAL RESULTS

Initial Streak Camera Data: As Found Steering

In order to investigate the short-range wakefield driven submicropulse effects, we used the HOM detector signals as a measure of how far off axis the beam was in the cavities. We initially used the beam transport as found with elevated HOM signals in both CC1 and CC2. We identified a y-t effect in the streak camera image shown in Fig. 2. The head of the pulse is lowest in the image so later time is upward. The projected bunch length is 11.2 ps (σ).
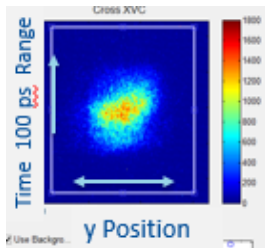
Figure 2: OTR streak camera Image at X121 with HOMs as found for Run 1.

The transport optics rotated the image 90° so we observed the y spatial information on the horizontal display axis as indicated. The temporal slices are shown in Fig. 3a for the head and tail of the pulses, and then Fig. 3b shows the Gaussian fits to three such profiles with a clear 343 μm shift of the centroid from head (blue curve) to tail (red curve). Based on the elevated HOM signals, we attribute the effects to a combination of both CC1 and CC2 wakefields.
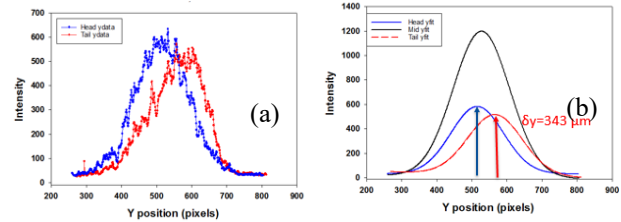

Figure 3: (a) Transverse profiles from the head and tail of the Fig. 2 Image (b) Gaussian fits to the transverse profiles taken at the head, middle, and tail of the longitudinal distribution. A head-to-tail centroid shift of 343 μm was observed.

We next steered the beam with the V103 corrector by ±2.4 A from the reference or ±4 mrad to evaluate the effects of CC2's wakefields. Interestingly, the +4 mrad steering almost doubled the head to tail centroid shift to +693 μm in Fig. 4b while the -4 mrad steering seemed to compensate the CC1 kick and reduced the centroid shift to -55 μm as shown in Fig. 4d. The projected beam size was also reduced.

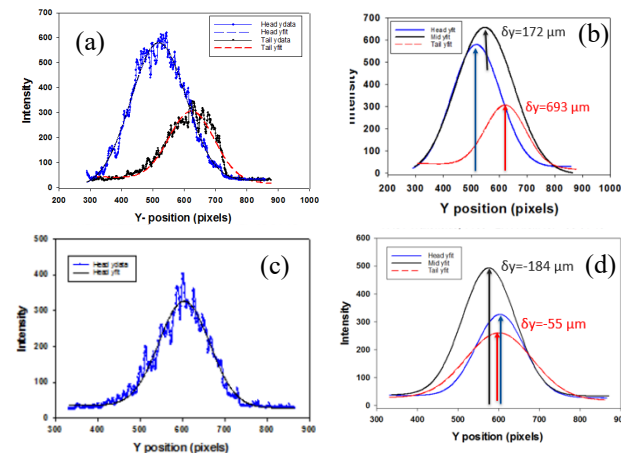Figure 4: (a) Transverse profiles from the head and tail of the image with V103= +2.4 A.(b) Gaussian fits to the transverse profiles taken at the head, middle, and tail of the longitudinal distribution. A head-to-tail centroid shift of 693 μm was observed. (c) Transverse profiles from the head and tail of the image with V103=-2.4A. (d) Gaussian fits to the transverse profiles taken at the head, middle, and tail of the longitudinal distribution. A head-to-tail centroid shift of only -55 μm was observed for this case.

Wake Fields and HOMs Minimized

The next run we used the H/V 101 correctors before CC1 and H/V 103 correctors before CC2 to minimize the four HOM signals at 500 pC/b and with 150 b. We observed an elliptical beam in y-t space as shown in Figure 5 as would be expected for a space-charge-dominated regime at the PC. In this case the laser spot size was ~ 0.2 mm as in the previous run. Also, we observe almost no y-t tilt during the micropulse so this looks like a preferred way to steer with the four HOM signals low at -13, -10, -5, -7 mV.
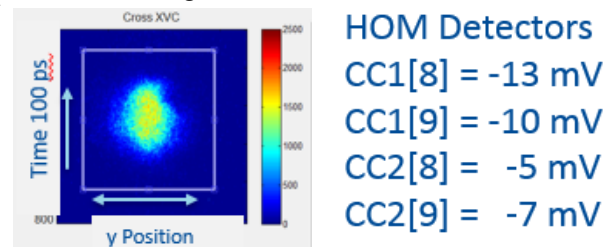

Figure 5: Streak camera y-t image at X121 that exhibits elliptical-shape effect with HOMs minimized.

In Fig. 6 we continued our studies, but we note the laser spot was now 1.2 mm RMS. Our HOM signal minima were not as low as in Fig. 5 with 500 pC/b, but we did observe a somewhat elliptical shape as shown in Fig. 6a. The beam size at the tail is much smaller than at the middle with no head-tail centroid shift. However, when we steered with V103 = -2A from the reference, we observed a clear 106-µm head-tail centroid shift and significant 139-µm profile size growth from the initial 224 µm at the tail. This would indicate significant dilution of slice emittance in that sample.
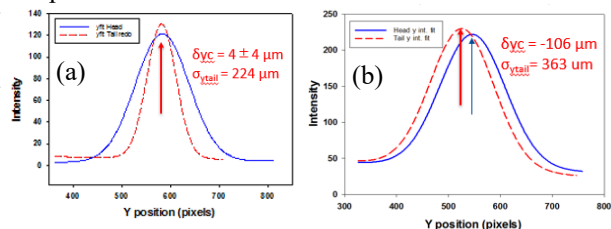

Figure 6: (a) Comparison of the Gaussian fits to the profile taken at the head and the tail of an image with HOMs minimized and laser spot of 1.1 mm RMS. (b) Comparison of the Gaussian fits to the profile taken at the head and the tail of an image with V103= -2A from reference. A clear centroid shift of -106 µm is seen, and a > 50 % larger profile at the tail is seen than in (a).

Bunch by Bunch rf BPM Data

We also evaluated the potential long-range wakefield or HOM effects on the beam centroid by using the rf BPM data. An example of the centroid motion within the 50-micropulse train of a macropulse is shown in Fig. 7 with both noise-reduction and bunch-by-bunch capabilities implemented.

The 100-kHz oscillation seen in the B117 data is a difference frequency between HOM mode 14 in CC2 and a beam harmonic [3]. The field oscillations kicked different micropulses varying amounts depending on the amplitude

at that point in time. The quadrupole triplet Q118-120 was used to focus the beam smaller in x while leaving the vertical size about 800 µm at the X121 station. The beam oscillation amplitude is much reduced to <20 µm at B121 downstream of these quadrupoles, and thus the main competing mechanism identified does not account for the observed y-t effect in the streak image. Since the numerical model for a TESLA cavity indicated a 100-120 µm head-tail kick for 500 pC/b and a 4-mm offset at 33 MeV [10], we attribute the 100-µm head-tail effects seen in Fig. 6 to predominately such short-range wakefields.
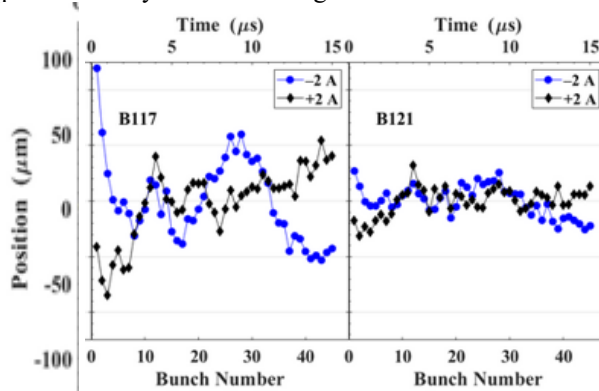

Figure 7: Examples of the variation of the beam vertical centroids bunch by bunch for 50 micropulses at B117 and B121 for V103 settings of ±2A from the reference. These were 100-shot averages to show the 100-kHz oscillation effects generated in CC2.

SUMMARY

In summary, a series of preliminary observations of short-range wakefield effects on beam dynamics were made using the streak camera to obtain y-t images at the submicropulse time scale. The HOM detectors and rf BPMs were used to evaluate off-axis steering related to these tests, and the HOM-induced sub-macropulse centroid motion was shown to be much smaller than the observed effects. Moreover, the head-tail centroid kicks were consistent with a short-range wakefield model for the TESLA-type superconducting rf cavity and attributed to that effect.

ACKNOWLEDGMENTS

The authors acknowledge the support of C. Drennan, A. Valishev, D. Broemmelsiek, G. Stancari, and M. Lindgren, all in the Accelerator Division at Fermilab.

REFERENCES

[1] H. Weise, "Commissioning and First Lasing of the European XFEL", in *Proc. FEL'17*, Santa Fe, NM, USA, Aug. 2017, pp. 9-13. doi:10.18429/JACoW-FEL2017-MOC03

[2] P. Emma, "Status of the LCLS-II FEL Project at SLAC", presented at *Proc. FEL'17*, MOD01, Santa Fe, NM, Aug. 2017, paper MOD01.

[3] A. H. Lumpkin *et al.,* "Submacropulse electron-beam dynamics correlated with higher-order modes in Tesla-type superconducting rf cavities", *Phys. Rev. Accel. and Beams*, vol. 21, p. 064401, 2018.

doi:10.1103/PhysRevAccelBeams.21.064401

[4] The ASTA User Facility Proposal, Fermilab-TM-2568, October 2013.

[5] J. Ruan, M. Church, D. Edstrom, T. Johnson, and J. Santucci, "Commission of the Drive Laser System for Advanced Superconducting Test Accelerator", in *Proc. IPAC'13*, Shanghai, China, May 2013, paper WEPME057, pp. 3061-3063.

[6] J. Diamond, FNAL, online Java-based ImageTool, 2013.

[7] R. Thurman-Keup, FNAL, off-line MATLAB-based ImageTool, 2011.

[8] A. H. Lumpkin, J. Ruan, and R. Thurman-Keup, "Synchroscan streak camera imaging at a 15-MeV photoinjector with emittance exchange", *Nucl. Instr. and Meth. A*, vol. 687, pp. 92-100, 2012.
doi: 10.1016/j.nima.2012.05.068

[9] A. H. Lumpkin, D. Edstrom, and J. Ruan, "Initial Demonstration of 9-MHz Framing Camera Rates", in *Proc. NAPAC'16*, Chicago, IL, USA, Oct. 2016, pp. 333-336.
doi:10.18429/JACoW-NAPAC2016-TUPOA25.

[10] V. Lebedev, private communication, May 2016.